ELSEVIER

Journal of Fluids and Structures 20 (2005) 345–357

JOURNAL OF FLUIDS AND STRUCTURES

www.elsevier.nl/locate/jnlabr/yjfls

Impact of a disk on shallow water

E.V. Ermanyuk[a,*], M. Ohkusu[b]

[a]*Lavrentyev Institute of Hydrodynamics, av. Lavrentyev 15, Novosibirsk 630090, Russian Federation*
[b]*Research Institute for Applied Mechanics, Kyushu University, Fukuoka, Japan*

Received 24 July 2002; accepted 24 October 2004

Abstract

This paper describes the experiments on shallow-water flat-bottom slamming of a circular disk. The dependence of the added mass of a disk on water depth and impact velocity is experimentally evaluated and compared with available theoretical predictions. The pressure time-histories at the bottom of the test tank are analyzed with the help of the wavelet transform technique. The wavelet spectra of the pressure records are shown to provide useful quantitative information on the significant time-scales of the impact phenomena. It is shown that the presence of an air cushion strongly affects the time-scale of impact and the splash-jet shape.
© 2004 Elsevier Ltd. All rights reserved.

1. Introduction

It is well known that impact of a body on the free surface is accompanied by significant hydrodynamic loads. Evaluation of the impact loading is of vital practical interest in many applications (slamming and planning of ships in rough sea, landing of airplanes on the water surface, etc.). When a falling body has a keel angle, the impact loads can be reliably estimated within the framework of classical studies by Pabst and Wagner dating back to the early 1930s. In the case of an arbitrary body geometry, the problem is quite complicated [see review by Korobkin and Pukhnachev (1988)]. In particular, impact of a body with a flat horizontal bottom on the water surface is accompanied by an air cushion effect. Owing to its complexity and practical importance, this phenomenon is a subject of ongoing theoretical and experimental research (see review in Mizoguchi and Tanizawa's review, 1996). For the particular case of a circular plate, the hydrodynamic loads were studied experimentally by Fujita (1954). The main effects of an air cushion on the impact loading were identified in the pioneering experimental study by Chuang (1966), whereas a rational theoretical approach to the problem was proposed in Verhagen (1967).

The above-mentioned studies were focused on impact phenomena in deep water. The effect of limited fluid depth has received little attention, in spite of its relevance to some practical problems such as planing in shallow water, collisions of lubricated mechanical parts of engines, etc. To our knowledge, the difference between deep-water and shallow-water cases has not yet been systematically studied in experiments.

The known theoretical literature on body impact onto shallow water is quite limited. Impact loading on a circular disk in water of finite depth was studied by Vorovich and Yudovich (1957). The water depth in their study was assumed to be sufficiently large. For shallow water, the hydrodynamic impact pressure on a disk was evaluated by Chebakov

*Corresponding author.
E-mail address: ermanyuk@hydro.nsc.ru (E.V. Ermanyuk).

0889-9746/$ - see front matter © 2004 Elsevier Ltd. All rights reserved.
doi:10.1016/j.jfluidstructs.2004.10.002

(1974) in the form of asymptotic series over a small parameter h/R, where h is the fluid depth, and R is the disk radius. Further theoretical developments in shallow-water impact problems are considered in Korobkin (1999).

The present paper describes an experimental study of the impact of a circular disk on shallow water. The measured values include the velocity of the body motion and the pressure at the bottom under the center of the falling disk. The data on the body velocity before and after the impact onto the free surface are used to evaluate the dependence of added mass on fluid depth, which is compared with theoretical predictions by Chebakov (1974). The pressure time-histories are analyzed with the help of wavelet transforms (Farge, 1992). The wavelet power spectra are shown to contain useful information about the dominant time-scales at different stages and conditions of impact. The dependence of the maximum impact pressure on water depth and impact velocity is obtained. The impact phenomenon is studied for two cases: (a) the falling disk collides with another disk lying on the water surface, and (b) the disk falls on the free surface.

It is known that in vacuum the characteristic time-scale for the impact loading on a flat-bottom body that falls on a free surface of deep water would be $2L/c_w$, where c_w is the speed of sound in water and L is the horizontal size of the body. The maximum impact pressure in this case is equal to the acoustic pressure $p_m = \rho_w c_w V_{-0}$, where ρ_w is the water density and V_{-0} is the body velocity just before the impact. However, in practice the maximum acoustic pressure never occurs because of the air cushion. In experiments (Chuang, 1966), the duration of the impact pressure (or half-period of pressure fluctuations of the trapped air region) for the case of flat-bottom slamming is found to be about $2L/c_a$, where c_a is the speed of sound in air. The maximum impact pressure p_m is found to be proportional to $\rho_w c_a V_{-0}$.

For shallow water, the existence of a small parameter h/R adds some new features to the impact phenomenon. In particular, at the initial (acoustic) stage, the shock wave generated due to body impact on the liquid surface may travel several times up and down, being reflected by the fluid bottom and the surface of the body. Thus, the acoustic stage can be characterized by three time-scales. Short time-scales, namely $2h/c_w$ and $4R/c_w$, characterize the passage of shock waves in water, while a longer time-scale $4R/c_a$ is associated with the air cushion. The velocity of the body motion undergoes a sharp change within a short period of contact with the free surface, the magnitude of this variation being dependent on the mass of the body M and the added mass μ, while the latter, in turn, is strongly dependent on h/R. The ratio $(V_{-0} - V_{+0})/V_{+0}$, where V_{+0} is the velocity of the body at the end of the acoustic stage, characterizes the loss of the body momentum due to collision with the surface of the water. In addition to the maximum impact pressure, the total impulse produced during the impact and the main time-scale of the impulse loading are believed to be of major importance from the viewpoint of structural damage and deflections.

At the inertial (hydraulic) stage of the impact, the flow of water from the gap between the fluid bottom and the bottom of the falling body undergoes a collision with otherwise quiescent fluid in the outer region. This collision leads to formation of a splash jet. Let us note that, since h/R is small, the presence of trapped air under the bottom can affect not only the acoustic stage of the impact but also the inertial stage. In the absence of an air cushion, the water flow depends solely on the variation of the distance between the body and the bottom. When an air cushion is present, the flow of water from the gap between the body and the bottom is also dependent on the motion of the trapped air. For typical experimental conditions, the time-scale of the inertial stage of impact, which can be represented as h/V_{+0}, is 1–2 orders of magnitude longer than the time-scale of the acoustic stage.

2. Experimental installation and procedure

The experiments were carried out at the Research Institute for Applied Mechanics, Kyushu University, in a test tank having the dimensions length × width × height = $1 \times 1 \times 0.2\,\mathrm{m}^3$. The scheme of the experimental setup is shown in Fig. 1. The walls and bottom of the test tank were made of acrylic glass. The bottom was reinforced by a metal structure. The center of the bottom was connected to a tube attached to the foundation. A pressure gauge of type PS-10 KA,C (KYOWA) with a maximum capacity 10^6 Pa and natural frequency 37 kHz was mounted at the bottom of the test tank inside the tube under the center of the falling body. The pressure time-history was recorded by an analog device having the high-pass frequency threshold of 20 kHz. Since the high-pass threshold is almost two times lower than the natural frequency of the pressure gauge, the natural oscillations of the pressure gauge should have been filtered out by the analog recording device. The analog records were sampled at the frequency 10 kHz by a 12-bit A/D converter.

The experimental set-up was designed to study the impact of a heavy disk (Disk 1) with and without the trapped air region in water. To avoid the presence of the trapped air region in water, a thin disk (Disk 2) was initially placed on the free surface. This experimental setup is hereinafter referred to as Case A. The mass m_1 of Disk 1 varied from 1 to 3 kg. The mass of Disk 2 was $m_2 = 0.22$ kg, i.e., m_2 was much smaller than m_1. The diameters of Disks 1 and 2 were $D = 0.2$ m. In Case A, a specific kind of air cushion occurs when air is forced to escape from the gap between Disks 1 and 2 during the impact. Since there is no trapped air region in water, the hydraulic stage in Case A is believed to be practically the same as in the idealized case of a body impact in vacuum.

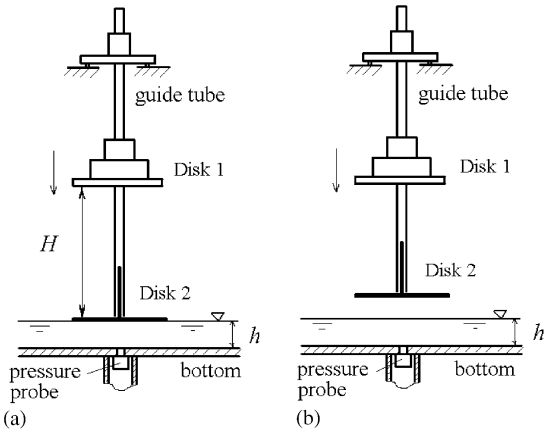

Fig. 1. Experimental set-up.

The experimental installation also enables the study of the conventional air cushion effect. To do this, Disk 2 was initially placed at a certain distance above the free surface. Disk 2 was held at an initial position by a weak spring placed inside the guiding tube. This experimental setup is hereinafter referred to as Case B. In the experiments, the distance between Disk 2 and the water surface was 0.03 m. The stiffness coefficient of the spring was $5.4\,\mathrm{Nm}^{-1}$. Since the elongation of the spring in the experiments did not exceed 0.05 m, the force due to the spring could be considered as constant, equal to $m_2 g$, where g is the acceleration due to gravity. Thus, the acceleration of the combined body of mass $m_1 + m_2$ due to this force was about $m_2 g/(m_1 + m_2)$. This value is fairly small compared to the acceleration at the acoustic and hydraulic stages of impact. In Case B, the presence of trapped air in shallow water could be expected to have significant effects both at the acoustic and hydraulic stages of impact. Thus, it is of interest to compare the effects of the air cushion between Disks 1 and 2 in Case A with the conventional air cushion effect in Case B.

The velocity of body motion was evaluated from the sequence of pulses produced by a photosensor, when a horizontal beam of light was crossed by a vertical pattern of black and white strips painted on a plate fixed to the falling body. The time span between two adjacent pulses corresponds to the time needed to change the vertical coordinate of the body by 5 mm. The method was tested by free-fall experiments performed in air. In Cases A and B, the drop height H was measured from the upper surface of the thin disk when it touched the water. The free-fall tests demonstrated that in Case A the velocity V_{-0} of Disk 1 just before the impact onto Disk 2 is smaller than the theoretical value because of friction, so that $V_{-0} = 0.96(gH)^{1/2}$. In Case B, the experimental impact velocity of the combined body Disk 1 plus Disk 2 was $V_{-0} = 0.93(gH)^{1/2} m_1/(m_1 + m_2)$, to within an accuracy of $\pm 2\%$. The measured decrease of velocity due to the collision between Disks 1 and 2 satisfied the law of momentum conservation for a nonelastic impact. Some additional decrease of the impact velocity was caused by the elastic spring supporting Disk 2.

3. Experimental results

3.1. Velocity of the disk at different stages of impact

A typical dependence of the body velocity V on the penetration depth b is shown in Fig. 2 for $h = 0.04$ m, $H = 0.15$ m and $m_1 = 2$ kg. The same data are replotted in Fig. 3 as the dependence of V on time t (the legend is the same as in Fig. 2). It is apparent that the impact phenomenon consists of two distinct stages. The duration of the initial (acoustic) stage can be roughly estimated as a few milliseconds, with corresponding negative acceleration almost two orders of magnitude higher than g (refined estimates based on the pressure time-histories are discussed later). The duration of the hydraulic stage of impact is of order 10^{-1} s. The negative acceleration of the falling body at the hydraulic stage is about 1 g, and it decreases with time. It is remarkable that the laws of the body motion at the hydraulic stage of impact are quite similar in both cases. However, it should be kept in mind that in Case B there is a region of trapped air under the bottom of the moving body. Correspondingly, for the same penetration depth of the disk, the actual water depth under the body in Case B is smaller than in Case A. As result, the inertial flow of water from beneath the body has higher velocities so that the conditions for formation of a splash jet in Cases A and B are quite different.

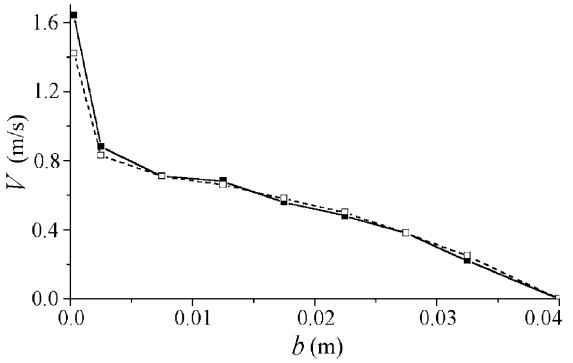

Fig. 2. Velocity versus penetration depth (■, Case A; □, Case B) for $h = 0.04\,\mathrm{m}$, $H = 0.15\,\mathrm{m}$, $M = 2\,\mathrm{kg}$.

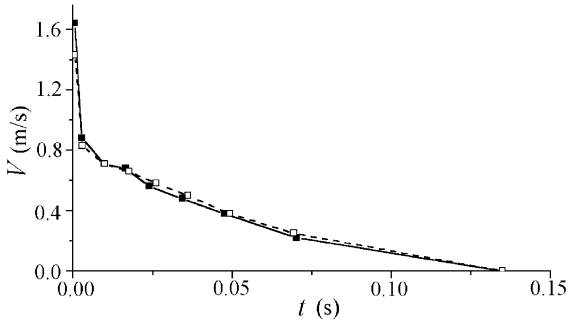

Fig. 3. Velocity versus time (■, Case A; □, Case B) for $h = 0.04\,\mathrm{m}$, $H = 0.15\,\mathrm{m}$, $M = 2\,\mathrm{kg}$.

3.2. Added mass

The concept of added mass has been effectively used in the theory of body impact on a free surface of a liquid. Indeed, the upward impact force F acting on a body moving with velocity V may be conveniently expressed in terms of the added mass μ as [see, for example, Moghisi and Squire (1981)]

$$F = \mathrm{d}(\mu V)/\mathrm{d}t \tag{1}$$

or, using the penetration depth, b, of the body under the undisturbed free surface, and taking into account $V = \mathrm{d}b/\mathrm{d}t$,

$$F = V^2 \frac{\mathrm{d}\mu}{\mathrm{d}b} + \mu \frac{\mathrm{d}V}{\mathrm{d}t}. \tag{2}$$

Usually, two typical cases are considered. For a heavy falling body with mass $M \gg \mu$ the variation of V during entry is negligibly small. Therefore, the second term in Eq. (2) can be neglected and one can assume $F = \frac{1}{2} C_d A \rho_w V^2$, where A is the cross-sectional area and the impact drag coefficient C_d is proportional to $\mathrm{d}\mu/\mathrm{d}b$. This case is considered, for example, in Moghisi and Squire (1981) (note that in their study the variation of V during entry was well below 1%). Another popular idealization is discussed in Batchelor (1967, Section 6.10), in relation to the normal impact of a flat-nosed body on a liquid half-space when the influence of the atmosphere is neglected. The displacement of the body at the moment of impact is assumed to be infinitely small. It is noted that the fluid motion produced by impact of the flat-nosed body is 'identical only instantaneously with that in one-half of the flow field of a flat plate moving through infinite fluid'. For application to the problem investigated in the present paper, the above considerations yield the large-depth limit ($h/R \to \infty$) of the added mass for the impact of a circular disk on a free surface as $\mu = (\frac{4}{3})\rho_w R^3$, which is one-half of the added mass for acceleration of a circular disk through infinite fluid in the direction of its axis (see Lamb, 1932). In what follows we assume the viewpoint taken in Batchelor (1967, Section 6.10). Applying the law of momentum conservation to the initial stage of the impact phenomenon, we can write $m_1 V_{-0} = (m_1 + m_2 + \mu) V_{+0}$ for Case A and

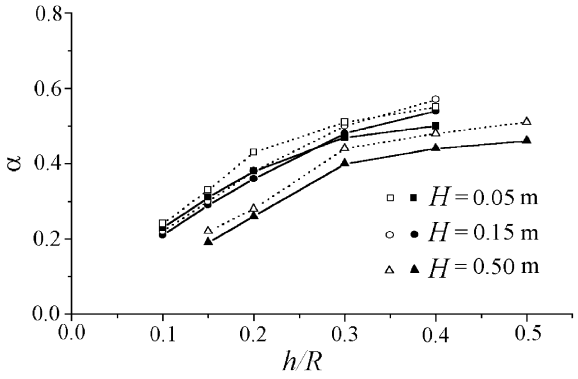

Fig. 4. Relative velocity drop $\alpha = V_{+0}/V_{-0}$ versus nondimensional fluid depth (■, ●, ▲, Case A; □, ○, △, Case B).

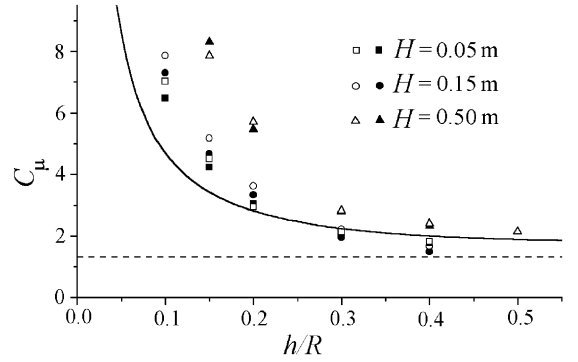

Fig. 5. Added mass coefficient versus nondimensional fluid depth (solid symbols: Case A; empty symbols: Case B; – – –, asymptotic value $C_\mu = \frac{4}{3}$ for $h/R \to \infty$).

$(m_1 + m_2)V_{-0} = (m_1 + m_2 + \mu)V_{+0}$ for Case B. Solving these equations for μ yields

$$\mu = \frac{m_1(1-\alpha)}{\alpha} - m_2 \quad \text{for Case } A, \tag{3}$$

$$\mu = \frac{(m_1 + m_2)(1-\alpha)}{\alpha} \quad \text{for Case } B \tag{4}$$

with $\alpha = V_{+0}/V_{-0}$.

In our experiments, the position of the photosensor that measured the displacement of the falling body was adjusted under static conditions so that the output signal changed when Disk 1 touched Disk 2 in Case A, or the lower surface of Disk 2 touched the water surface in Case B. The mean velocity of the body over displacement $\delta = 5\,\text{mm}$ after the impact is taken as V_{+0}. It should be kept in mind that this definition leads to somewhat underestimated values of V_{+0}. The experimentally measured $\alpha(h/R)$ dependencies for different impact heights H are plotted in Fig. 4. For the data, shown in Fig. 4, $M = 2\,\text{kg}$. Using (3) and (4), the data for $\alpha(h/R)$ are replotted in Fig. 5 to show the dependence of the added mass coefficient $C_\mu = \mu/\rho_w R^3$ on h/R for different drop heights H. The solid line in Fig. 5 corresponds to the theoretical dependence given in Chebakov (1974)

$$C_\mu = \frac{\pi}{8}\left(\frac{h}{R}\right)^{-1} + \frac{\ln 4}{2} + \frac{(\pi^2 + 3\ln^2 4)}{6\pi}\left(\frac{h}{R}\right) - \text{h.o.t.}, \tag{5}$$

where h.o.t. denotes the high-order terms which are to be taken into account when $h/R > 0.5$. In general, the above dependence is in good quantitative agreement with the experimental data obtained at the lowest experimental drop height $H = 0.05\,\text{m}$. However, the higher the drop height, the lower is α (Fig. 4) and the greater is C_μ (Fig. 5). Hence, we

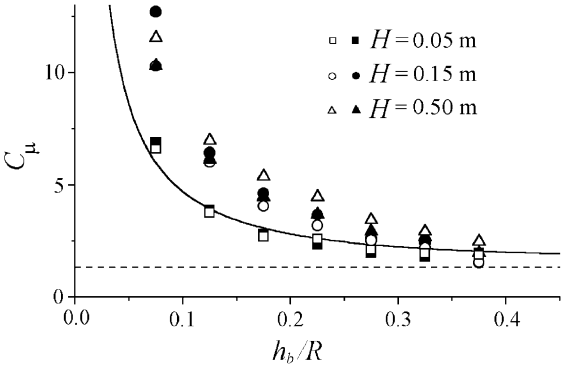

Fig. 6. Added mass coefficient versus instantaneous nondimensional fluid depth ($h = 0.04$ m, $R = 0.1$ m, legend and symbols are the same as in Fig. 5).

can conclude that nonlinear effects are important for high impact velocities. It is remarkable that the difference between the values of C_μ measured in Cases A and B is relatively low. As h/R increases, the added mass coefficient approaches $C_\mu(\infty) = \frac{4}{3}$ which is shown in Fig. 5 by a dashed line.

The above considerations are focused on evaluation of $C_\mu(h/R)$ during the impact when the penetration b is small (in practice, we used the data for b in the range $0 < b \leqslant \delta$). It is interesting to evaluate the variation of the added mass as a function of $h_b = h - b$ during the hydraulic stage of impact for $0 < b < h$. Neglecting gravity and following Moghisi and Squire (1981, Section 2), we can write the force acting on a free body of mass M as

$$-F = \mathrm{d}(MV)/\mathrm{d}t. \tag{6}$$

Equating (6) and the hydrodynamic force (1) yields $(\mathrm{d}/\mathrm{d}t)[(\mu + M)V] = 0$, which, after integration, gives

$$V/V_{-0} = M/(\mu + M). \tag{7}$$

Thus, if we know the added mass as a function of $\mu(t)$ or $\mu(b)$, we can estimate the velocity as function $V(t)$ or $V(b)$ and vice versa. Taking into account that in Case A the falling mass is $M = m_1$ and m_2 should be added to μ, while in Case B the falling mass is $M = m_1 + m_2$, we can estimate $\mu(h_b)$ from the data on $V(h_b)$ (a sample of $V(b)$ is shown in Fig. 2). Such an estimate is presented in Fig. 6 for Case A (black symbols) and Case B (open symbols) at fixed initial fluid depth $h = 0.04$ m and different initial impact heights H. The dependence given by Eq. (5) with h replaced by h_b is shown by the solid line. One can see good quantitative agreement between this dependence and the experimental points obtained at $H = 0.05$ m. Thus, at least at low impact velocity, added mass predicted by Eq. (5) can be used in Eq. (7) for the prediction of the body motion at the hydraulic stage of impact. At high impact velocity the behavior of the added mass is qualitatively the same as in Fig. 5.

Physically, the increase of the apparent added mass for high impact velocities may mean that the kinetic energy of the falling body is transformed not only into the kinetic energy of the fluid motion as assumed in Chebakov (1974) but also into the energy of compressed air motion, acoustic energy, etc. Another, and probably, more important, reason for the apparent growth of added mass with the impact velocity is the finite value of δ used in the experiments for evaluation of α. Indeed, in the theory of impulsive motion of a fluid it is usually assumed (Batchelor, 1967) that the displacement of a body during impulse is negligibly small and in the equations of fluid motion the terms involving fluid velocities and their spatial gradients are small compared to the local acceleration of fluid particles. These assumptions are violated when we consider finite δ comparable with h and $h/R \to 0$. Accordingly, nonlinear effects become increasingly important for high impact velocities (especially when $\mathrm{d}\mu/\mathrm{d}b$ is large). In this situation, it is difficult to formulate a rigorous method for experimental evaluation of the added mass.

3.3. Analysis of the pressure time-history

Within the past two decades, the wavelet transform technique has been successfully applied in different hydrodynamic problems (a detailed review is given in Farge, 1992). Wavelet transforms are recognized as an effective tool for the analysis of complicated phenomena characterized by time-evolution of local time-scales. In the present, paper we apply this technique to flat-bottom slamming in shallow water.

First, let us introduce the analyzing wavelets $\psi(T,\tau,t)$ generated by dilations T and translations τ from the mother wavelet $\psi(t)$, so that

$$\psi(T,\tau,t)=\frac{1}{\sqrt{T}}\,\psi\Big(\frac{t-\tau}{T}\Big).$$

The function $\psi(t)$ should satisfy the following admissibility condition:

$$\int_{-\infty}^{\infty}|\widehat{\psi}(\omega))|^2|\omega|^{-1}\,\mathrm{d}\omega<\infty,$$

where $\widehat{\psi}(\omega)$ is the Fourier transform of $\psi(t)$:

$$\widehat{\psi}(\omega)=\frac{1}{2\pi}\int_{-\infty}^{\infty}\psi(t)\mathrm{e}^{-\mathrm{i}\omega t}\,\mathrm{d}t.$$

The wavelet transform of a time-series $p(t)$ is defined as the inner product of $\psi(T,\tau,t)$ and $p(t)$:

$$\widetilde{p}(T,\tau)=\langle\psi(T,\tau,t),p(t)\rangle=\int_{-\infty}^{\infty}p(t)\psi^*(T,\tau,t)\,\mathrm{d}t,$$

where asterisk denotes the complex conjugate. The properties of wavelet transforms are discussed in Farge (1992). By analogy with the Fourier energy density spectrum, we can introduce a wavelet spectrum for a data series $p(t)$ as

$$E(T,\tau)=\widetilde{p}(T,\tau)\widetilde{p}^*(T,\tau)/T^2=|\widetilde{p}(T,\tau)|^2/T^2.$$

In the present paper, we use a complex-valued mother wavelet, which represents a plane wave modulated by a Gaussian envelope (the so-called Morlet wavelet):

$$\psi(t)=\mathrm{e}^{\mathrm{i}2\pi t}\mathrm{e}^{-t^2/2}.$$

For $\widetilde{p}(T,\tau)$ obtained with the help of the Morlet wavelet, the time-scale T has the physical sense of a local period of $p(t)$ at time-instant τ. For fixed $\tau=\tau_0$, the wavelet spectrum $E(T,\tau_0)$ reflects the local distribution of energy between different time-scales. Since the local distribution $E(T,\tau_0)$ is not necessarily representative for the whole process, one can introduce also the integral distribution for the studied range of time $0<\tau<\tau_{\max}$

$$\bar{E}(T)=\int_0^{\tau_{\max}}E(T,\tau)\,\mathrm{d}\tau.$$

Typical time-histories of pressure at the bottom of the test tank at the acoustic stage of impact are shown in Figs. 7(a) and 8(a) for Cases A and B, respectively. The experimental parameters for these records are: $H=0.05\,\mathrm{m}$, $h=0.02\,\mathrm{m}$, $M=2\,\mathrm{kg}$. It is apparent that the time-scales and the maximum values of pressures for Cases A and B are quite different. In particular, the main pressure peak in Case A is much sharper than in Case B. The pressure fluctuations that follow the main pressure peak in Case A have shorter time-scale and persist for a shorter time than in Case B. The quantitative information and the details of the process can be inferred from the contour map of the wavelet spectrum $E_n(T,\tau)$ (Figs. 7(b) and 8(b)), its cross-sections $E_n(T,\tau_i)$ at different moments of time τ_i (Figs. 7(c) and 8(c)) and the integral spectrum $\bar{E}_n(T)$, where the subscript n denotes the wavelet spectra normalized by their peak values, i.e., $E_n(T,\tau)=E(T,\tau)/\max[E(T,\tau)]$ and $\bar{E}_n(T)=\bar{E}(T)/\max[\bar{E}(T)]$.

In Case A (see Fig. 7(b)), the main time-scale that corresponds to the maximum of the wavelet spectrum is $T_0=7\times10^{-4}\,\mathrm{s}$. Presumably, this time-scale is defined by the effect of air flow from the gap between Disks 1 and 2 during the collision. Let us denote as τ_0 the time instant corresponding to the maximum of $E_n(T,\tau)$. Fig. 7(c) shows the cross-sections of $E_n(T,\tau)$ at τ_0, $\tau_1=\tau_0+3\times10^{-4}\,\mathrm{s}$ and $\tau_2=\tau_0+6\times10^{-4}\,\mathrm{s}$. One can see that the energy content at the time-scale T_0 decays with time very fast. The pressure fluctuations that follow the main pressure peak occur at the time-scale $T_*\simeq4\times10^{-4}\,\mathrm{s}$. The fluctuations at the time-scale between 4×10^{-4} and $5\times10^{-4}\,\mathrm{s}$ are typically detectable for the local and integral wavelet spectra obtained in Case A. It is quite difficult to identify the physical nature of the pressure fluctuations at this time-scale. However, since the time-scale is quite short, we can make a conjecture that it might be a multiple of the time-scale for relaxation of sound waves in water. The time-scale associated with propagation of the shock waves in water between the body and the bottom of the test tank, namely, $2h/c_w$ is too short to be detected by the measuring system used in our experiments. The relaxation time for the shock waves in water is related to the longer time-scale given by the time the sound needs to travel from one edge of the disk to the other and back, that is $4R/c_w=2.8\times10^{-4}\,\mathrm{s}$, where the speed of sound in water is taken as $c_w=1450\,\mathrm{m/s}$.

In Case B (see Fig. 8(b)), the main time-scale corresponding to the maximum of the wavelet spectrum is $T_0=18\times10^{-4}\,\mathrm{s}$. This time-scale is clearly associated with oscillations of the trapped air region. Hence, we can evaluate the

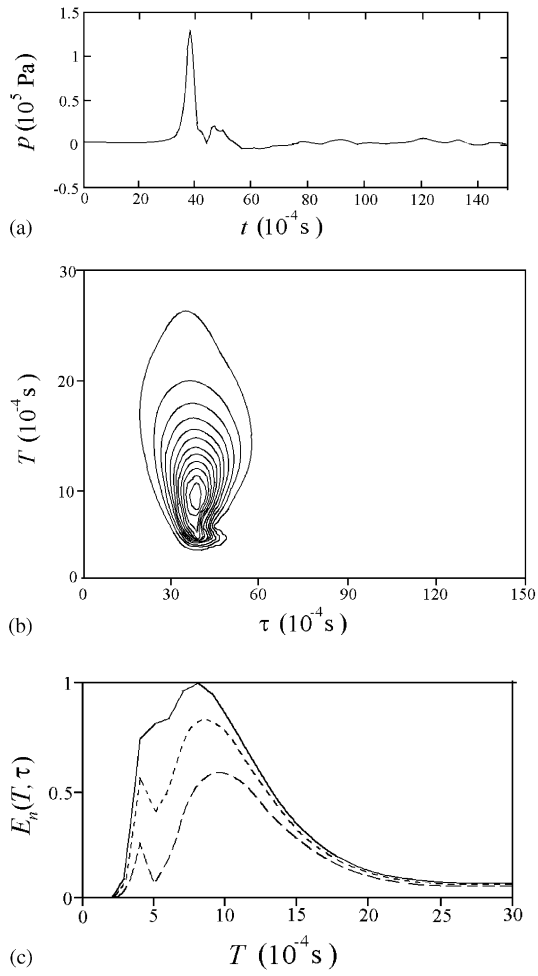

Fig. 7. (a) Pressure time-history, (b) contour map of wavelet spectrum $E_n(T,\tau)$ (12 contours between $E_n(T,\tau)=0$ and $E_n(T,\tau)=1$), (c) local wavelet spectra $E_n(T,\tau)$ for $\tau=\tau_0$ (—), $\tau=\tau_1=\tau_0+\Delta\tau$ (- - - -), $\tau=\tau_2=\tau_0+2\Delta\tau$ (— — —), with $\Delta\tau=3\times10^{-4}$ s. Case A ($h=0.02$ m, $H=0.05$ m, $M=2$ kg).

horizontal half-size of this region as $l=(c_aT_0)/8$. The present experiments were conducted at a temperature of about 18 °C. Correspondingly, the speed of sound in air at this temperature is about 340 m/s. Thus, the horizontal half-size of the trapped air region is $l=0.77R$. This size is fairly constant at all experimental conditions studied. As is seen in Fig. 8(b), at large τ the 'tail' corresponding to the main time-scale of the pressure oscillations is bent toward lower values of T. In Fig. 8(c) this effect is illustrated by cross-sections of the energy spectrum taken at the moments τ_0 corresponding to the maximum of $E_n(T,\tau)$, $\tau_1=\tau_0+3\times10^{-3}$ and $\tau_2=\tau_0+6\times10^{-3}$ s. The shift between the maxima of $E_n(T,\tau_2)$ and $E_n(T,\tau_1)$ is clearly seen. This effect was observed for the wavelet spectra of all experimental records $p(t)$. It seems physically reasonable to assume that decrease of the period of pressure oscillations is caused by decrease of the trapped air region with time.

In the present study, we are primarily concerned with the effects of limited water depth on the impact phenomenon. The wavelet technique allows one to analyze the energy distribution over different time-scales at different h/R. An example is presented in Fig. 9(a) and (b) (Case A) and Fig. 10(a) and (b) (Case B) for $H=0.05$ m and $M=2$ kg. The upper curves in Figs. 9 and 10 correspond to local wavelet spectra $E_n(T,\tau_0)$, while the lower curves show the integral spectra $\bar{E}_n(T)$.

In Case A (Fig. 9) there is no clear trend in the shape of the wavelet spectra corresponding to different h/R. The maxima of local spectra $E_n(T,\tau_0)$ are located at T_0, which varies between 7×10^{-4} and 8×10^{-4} s. A secondary peak occurs at the time-scale 4×10^{-4} s. The main peaks of the integral wavelet spectra $\bar{E}_n(T)$ at different h/R are located at the same time-scale $T_0=10^{-3}$ s.

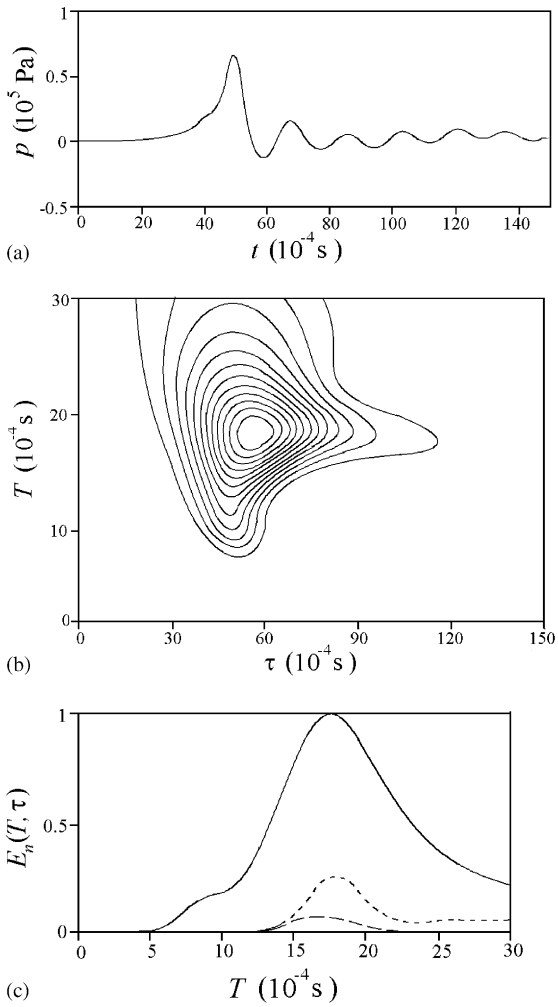

Fig. 8. (a) Pressure time-history, (b) contour map of wavelet spectrum $E_n(T,\tau)$ (12 contours between $E_n(T,\tau)=0$ and $E_n(T,\tau)=1$), (c) local wavelet spectrum $E_n(T,\tau)$ for $\tau=\tau_0$ (—), $\tau=\tau_1=\tau_0+\Delta\tau$ (----), $\tau=\tau_2=\tau_0+2\Delta\tau$ (– – –), with $\Delta\tau=3\times10^{-3}$ s. Case B ($h=0.02$ m, $H=0.05$ m, $M=2$ kg).

In Case B (Fig. 10) there exists a pronounced systematic variation of dominant time-scales with h/R. At $h/R=0.2$ the peak values of the local and integral spectra are located at $T_0=1.8\times10^{-3}$ s. However, at $h/R=0.05$ the main maximum of the local spectrum shifts to $T_0=10^{-3}$ s, i.e., it practically coincides with the main time-scale for Case A. The integral spectra (Fig. 10(b)) also show the increase of the energy content at short time-scales when h/R decreases.

Based on the above considerations we can draw some important conclusions. As is shown in Figs. 4 and 5, there is relatively little difference between α and C_μ measured in Cases A and B. However, another dynamically important quantity, namely, the acceleration of a body at the moment of impact evaluated as $(V_{-0}-V_{+0})/T_*$, where T_* is the impact time-scale, is strongly sensitive to the value of T_*. The evaluation of significant time-scales in Cases A and B show that Case A yields an upper bound on dynamic parameters (acceleration and pressures) due to the impact phenomenon. Importantly, the boundary conditions in Case A are much simpler for a theoretical treatment than the complicated conditions on the free surface in Case B. Thus, Case A can serve as a simple model for evaluation of the air cushion effect in shallow water. In theoretical analysis, Disk 2 can be replaced by a fictitious rigid weightless body. Moreover, as apparent from comparison between Figs. 9 and 10, as h/R decreases the significant time-scale in Case B shifts toward the significant time-scale of Case A. Correspondingly, at very low h/R the main parameters of the impact loading, namely, the body acceleration and maximum impact pressure should be practically the same in both cases. This conjecture is supported by Fig. 11 that shows the measured values of the maximum impact pressure p_m at the bottom of

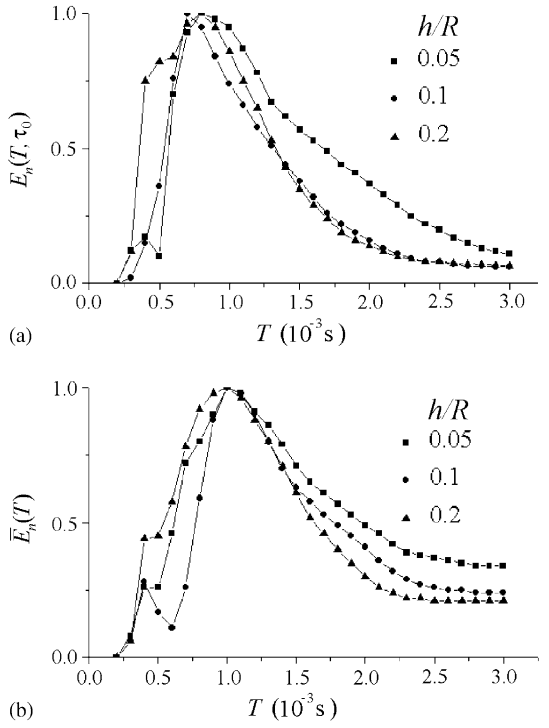

Fig. 9. (a) Local wavelet spectra at $\tau = \tau_0$, and (b) integral wavelet spectra ($H = 0.05\,\mathrm{m}$, $M = 2\,\mathrm{kg}$); Case A.

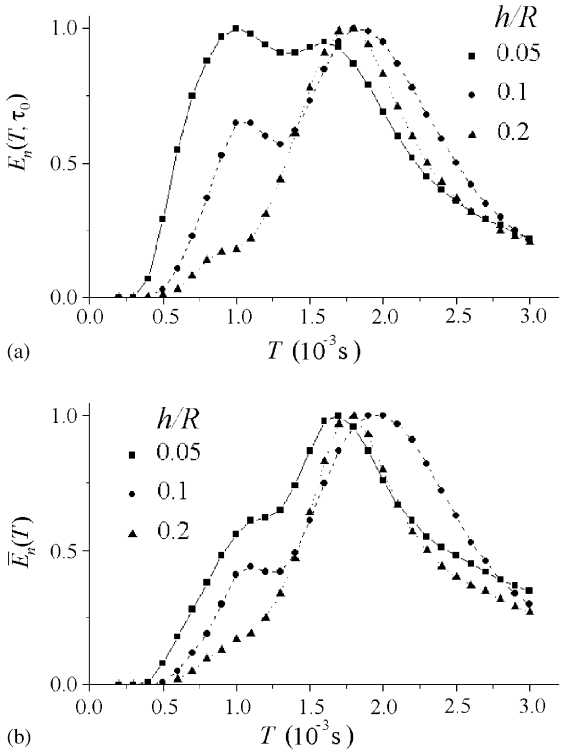

Fig. 10. (a) Local wavelet spectra at $\tau = \tau_0$, and (b) integral wavelet spectra ($H = 0.05\,\mathrm{m}$, $M = 2\,\mathrm{kg}$); Case B.

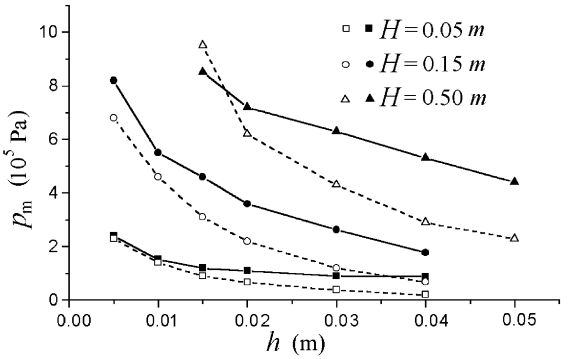

Fig. 11. Maximum impact pressure versus fluid depth (solid symbols: Case A; empty symbols: Case B).

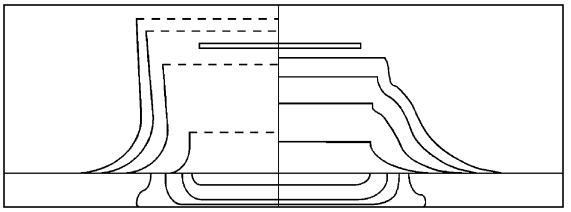

Fig. 12. Splash jet contours ($\Delta t = \frac{1}{30}$ s), rectangle shows the initial position and horizontal size of Disk 1 (right side: Case A; left side: Case B), $h = 0.04$ m, $H = 0.15$ m, $M = 2$ kg.

the test tank under the center of the falling disk. The data were obtained for $M = 2$ kg. One can see that the difference between the values of p_m measured in Cases A and B decreases for lower values of the water depth h. The data shown in Fig. 11 were also analyzed to obtain the dependence of the maximum pressure p_m on the impact velocity V_{-0}. It was found that $p_m \sim V_{-0}^{1.6}$ in Case A and $p_m \sim V_{-0}^{2.1}$ in Case B, i.e., the nonlinear effects at high impact velocities are more pronounced in Case B.

Although, in the present experiments the acceleration of Disk 1 at the acoustic stage of impact was not measured, a reliable order-of-magnitude estimate, namely, $(V_{-0} - V_{+0})/T_*$, can be easily obtained from the information about the added mass and significant time-scales presented in this section. The acceleration at the hydraulic stage can be roughly estimated as $V_{+0}^2/(2h)$.

3.4. Splash-jet shape

As has already been mentioned, the presence of a trapped air region under the bottom of the falling disk may affect both the acoustic and the hydraulic stages of the impact phenomenon. In this section, we consider the hydraulic stage and present some observations concerning the formation of the splash jet. The time-evolution of the jet contour was obtained from video records of the impact. The shape of the splash jet generated by the falling body is illustrated in Figs. 12 and 13 for $h/R = 0.4$ and 0.15, with the time-span between the successive frames $\Delta t = \frac{1}{30}$ s and $\Delta t = \frac{1}{60}$ s, respectively. In all cases the drop height was $H = 0.15$ m and the mass of the falling body was $M = 2$ kg. The right- and left-hand sides of the figures correspond to Cases A and B, respectively. As apparent, the presence of the trapped air region under the bottom of the disk produces a drastic change of the jet shape. In Case A (see Fig. 12) the jet is inclined toward the falling body as it might be expected from the theoretical considerations presented in Korobkin (1999). In Case B the outer contour of the jet is almost vertical with a slight inclination in outward direction. Also, in Case B the jet has smaller thickness than in Case A and propagates with higher velocity. For high velocity of water particles and small jet thickness, the capillary instability at the jet tip is quite pronounced. For this reason, the upper circumference of the jet in Case B (Figs. 12 and 13) and Case A (Fig. 13) is depicted by a horizontal dash line that represents merely a certain 'mean' elevation of the jet tip. In reality, the circumference of the jet tip is 'crown'-shaped. The instabilities at the jet tip were quite weak for $h = 0.04$ m in Case A so that the jet elevation could be determined with a good precision.

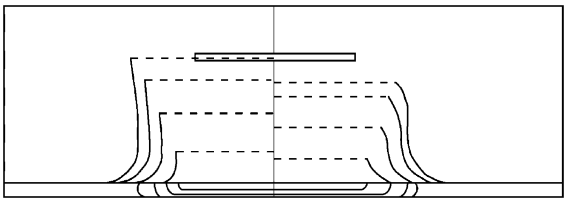

Fig. 13. Splash jet contours ($\Delta t = \frac{1}{60}$ s), rectangle shows the initial position and horizontal size of Disk 1 (right side: Case A, left side: Case B), $h = 0.015$ m, $H = 0.15$ m, $M = 2$ kg.

Correspondingly, in the right-hand side of Fig. 12 the horizontal projection of the upper circumference of the jet is depicted by a solid line.

It is pertinent to make a reference to the experimental study reported in Yakimov (1973). These experiments were concerned with the effect of the air density on the shape of a jet produced by impact of a body onto a free surface of water. The air density was changed by reducing the pressure in the experimental installation. The shape of the splash jet was shown to be strongly dependent on the air density. In the present study, we have shown that the mere fact of presence or absence of a trapped air region under the bottom of the falling body has a pronounced effect on the shape and dynamics of the splash jet. We can presume that the jet observed in Case A in our experiments is similar to the one that could be observed in vacuum.

The comparison of Figs. 12 and 13 shows that the qualitative difference between the splash jets in Cases A and B becomes less pronounced as the water depth decreases.

As can be seen in Figs. 12 and 13, at the final stage of impact, i.e., when the disk touches the bottom of the test tank, it is surrounded by a 'dry-bottom' region with the radius about $1.7R$, which was fairly constant for all the experimental conditions studied. When this size is reached, the 'dry-bottom' region starts to collapse. This observation may be of importance for realistic specification of initial conditions in the theoretical and numerical models of possible wave effects due to the impact of large bodies, say, meteorites, in shallow-water regions. Let us note that similar effects for the 2-D case are discussed by Bukreev and Gusev (1996) in their experimental study focused on wave effects due to the fall of a body on water of limited depth.

4. Conclusions

This paper deals with an experimental study of impact of a circular disk on shallow water. The experiments were performed for conventional slamming, with a region of trapped air under the bottom of the falling flat-bottom disk; and for the case of a disk impacting on a thin plate floating on the water surface. The latter case was found to be characterized by shorter time-scales and higher amplitudes of the impact loads. It is shown that at low impact velocity the experimentally evaluated added mass agrees well with theoretical predictions for the normal impact of a flat-nosed body on an ideal incompressible fluid, with the effects of atmosphere neglected. For high impact velocity, nonlinear effects become increasingly important, leading to a substantial increase of the apparent added mass.

The records of the impact-pressure at the bottom of the test tank have been analyzed with the help of wavelet transforms. The time-scale of the pressure pulsations in the trapped-air region is found to be fairly constant over a wide range of experimental parameters, yielding the estimated horizontal half-size of the trapped-air region as about 0.77 of the disk radius. It has been observed that in the studied range of experimental parameters at the final stage of impact, when the disk touches the bottom, it is surrounded by a dry-bottom region with a radius of around 1.7 of the disk radius.

Acknowledgements

The authors are grateful to Mr Inada and Mr Yasunaga for their help in experiments and inventive mechanical work. Thanks are due to Prof. A. Korobkin for interesting and fruitful discussions. The first author gratefully acknowledges his appointment as a visiting researcher at RIAM in summer 1998—spring 1999. The first author is also thankful to the Science Support Foundation for partial support.

References

Batchelor, G.K., 1967. An Introduction to Fluid Dynamics. Cambridge University Press, Cambridge.
Bukreev, V.I., Gusev, A.V., 1996. Gravity waves generated by a body falling onto shallow water. Journal of Applied Mechanics and Technical Physics 32, 224–231.
Chebakov, M.I., 1974. Circular disk impact on liquid of small depth. Prikladnaya Matematika i Mekhanika 38, 675–681 (in Russian).
Chuang, S.-L., 1966. Experiments on flat-bottom slamming. Journal of Ship Research 10, 10–17.
Fujita, Y., 1954. Impact of circular plate falling upon a water surface. Journal of the Society of Naval Architects of Japan 94, 105–110.
Farge, M., 1992. Wavelet transforms and their applications to turbulence. Annual Review of Fluid Mechanics 24, 395–457.
Korobkin, A.A., 1999. Shallow-water impact problems. Journal of Engineering Mathematics 35, 233–250.
Korobkin, A.A., Pukhnachev, V.V., 1988. Initial stage of water impact. Annual Review of Fluid Mechanics 20, 159–186.
Lamb, H., 1932. Hydrodynamics. Cambridge University Press, Cambridge.
Mizoguchi, S., Tanizawa, K., 1996. Impact wave loads due to slamming—a review. Ship Technology Research 43, 139–151.
Moghisi, M., Squire, P.T., 1981. An experimental investigation of the initial force of impact on a sphere striking a liquid surface. Journal of Fluid Mechanics 108, 133–146.
Verhagen, J.H.G., 1967. The impact of a flat plate on a water surface. Journal of Ship Research 10, 211–223.
Vorovich, I.I., Yudovich, V.I., 1957. Circular disk impact on liquid of finite depth. Prikladnaya Matematika i Mekhanika 21, 525–532 (in Russian).
Yakimov, Yu.L., 1973. Effect of the atmosphere with the fall of bodies into water. Fluid Dynamics 8, 679–682.